

# Atom-Resolved Imaging of Dynamic Shape Changes in Supported Copper Nanocrystals

Poul L. Hansen,<sup>1\*</sup> Jakob B. Wagner,<sup>1,2</sup> Stig Helveg,<sup>1</sup>  
Jens R. Rostrup-Nielsen,<sup>1</sup> Bjerne S. Clausen,<sup>1</sup> Henrik Topsøe<sup>1</sup>

In situ transmission electron microscopy is used to obtain atom-resolved images of copper nanocrystals on different supports. These are catalysts for methanol synthesis and hydrocarbon conversion processes for fuel cells. The nanocrystals undergo dynamic reversible shape changes in response to changes in the gaseous environment. For zinc oxide-supported samples, the changes are caused both by adsorbate-induced changes in surface energies and by changes in the interfacial energy. For copper nanocrystals supported on silica, the support has negligible influence on the structure. Nanoparticle dynamics must be included in the description of catalytic and other properties of nanomaterials. In situ microscopy offers possibilities for obtaining the relevant atomic-scale insight.

The size, shape, and structure of a nanomaterial affect its catalytic, optical, and electronic properties in ways that are difficult to predict (1–4). Procedures for synthesis of nanoparticles with well-defined shapes offer possibilities for addressing these issues (1–4). The stability of the synthesized shapes is not, however, guaranteed. In situ studies of metallic nanoparticles for applications in catalysis have shown that the state of the material may change from the as-synthesized state and may depend on the conditions en-

countered during catalysis (5–9). In situ spectroscopic methods now allow direct investigations of the nanoparticles (10–15) under catalytic relevant conditions, but complementary atomic-level, real-space information on the dynamic structure and morphology changes of metallic particles under similar conditions has not been available (16).

Transmission electron microscopy (TEM) provides real-space images with a resolution of down to 0.1 nm. However, TEM has been used mainly for ex situ studies of the atomic structure of supported nanoparticles after various treatments (17–21). In the first in situ TEM study (22) of catalysts in a reactive gas at elevated temperature, the resolution was about 2 nm. Later developments have demonstrated a

resolution down to 0.23 nm (23), allowing imaging of the largest lattice spacing in noble metals such as Pt (23) and Ru (9). To get detailed structural information on important catalytic metals, such as Fe, Ni, and Cu, a resolution of at least 0.18 nm is required. Here, we used a recently developed in situ TEM facility (9), which after some further modifications provides image resolution of about 0.14 nm during exposure of the sample to reactive gases and elevated temperatures.

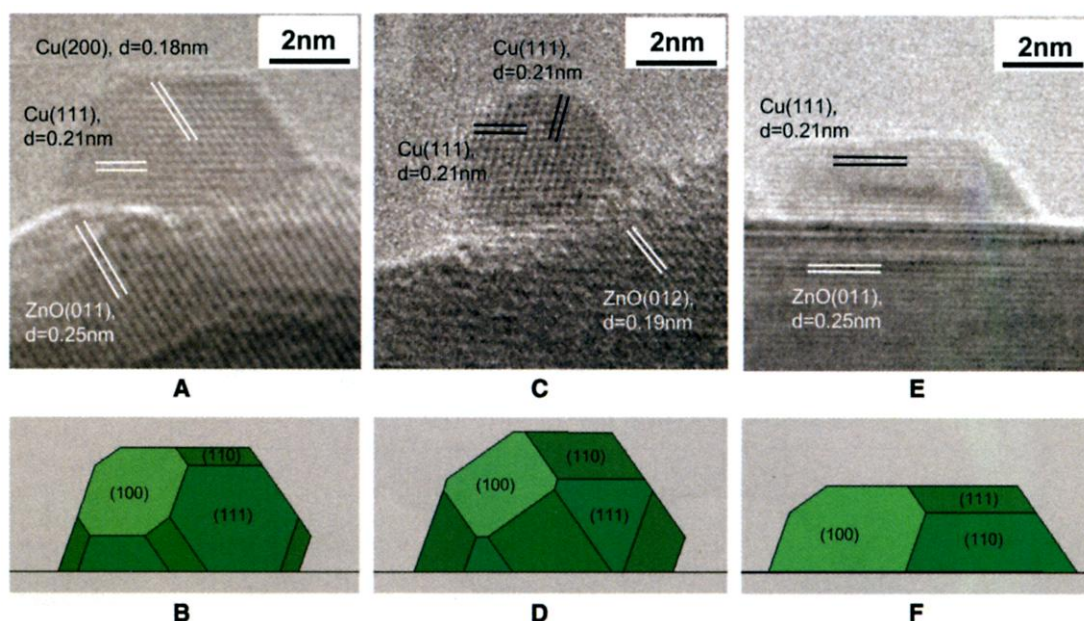
In the following, we focus on Cu nanoparticles with diameters of 3 to 6 nm dispersed on ZnO and silica supports. The Cu/ZnO system represents the industrial methanol synthesis catalyst (24). This system is also attracting interest in connection with conversion of hydrocarbons and alcohols for fuel cells (25), and the methanol synthesis reaction has been considered a prototype reaction for understanding complex metal/support interactions. Previous in situ extended x-ray absorption fine structure, x-ray diffraction, and Fourier transform infrared experiments on Cu/ZnO methanol synthesis catalysts (6–8, 26–28) have shown that the structure and catalytic activities of the Cu particles are strongly influenced by the gaseous environment (6–8, 26, 28). The effects appear to be dependent on the nature of the support because silica-supported Cu particles exhibit different behavior (6, 26).

Model catalysts were prepared by impregnation of a ZnO or silica support with an aqueous solution of Cu-acetate (29). The Cu metal nanocrystals were produced in situ by reduction of the CuO precursor in pure hydrogen for 1 hour at about 5-mbar pressure and at a temperature of 280°C. TEM images such as Fig. 1A confirm the presence of

<sup>1</sup>Haldor Topsøe A/S, Nymøllevej 55, DK-2800 Kgs. Lyngby, Denmark. <sup>2</sup>NBIFAFG, University of Copenhagen, Universitetsparken 5, DK-2100 Copenhagen Ø, Denmark.

\*To whom correspondence should be addressed. E-mail: plh@topsoe.dk

**Fig. 1.** In situ TEM images (A, C, and E) of a Cu/ZnO catalyst in various gas environments together with the corresponding Wulff constructions of the Cu nanocrystals (B, D, and F). (A) The image was recorded at a pressure of 1.5 mbar of H<sub>2</sub> at 220°C. The electron beam is parallel to the [011] zone axis of copper. (C) Obtained in a gas mixture of H<sub>2</sub> and H<sub>2</sub>O, H<sub>2</sub>:H<sub>2</sub>O = 3:1 at a total pressure of 1.5 mbar at 220°C. (E) Obtained in a gas mixture of H<sub>2</sub> (95%) and CO (5%) at a total pressure of 5 mbar at 220°C.



metallic Cu particles on both supports. To study the response of the Cu particles to variations in the gas composition, we exposed the catalyst to more oxidizing conditions by adding H<sub>2</sub>O to the hydrogen gas (Fig. 1C) and reducing conditions by adding CO to the hydrogen gas (Fig. 1E). Upon each change in gas composition, the particles changed their shape. Images were recorded during these dynamic changes. The pictures shown in Fig. 1, A, C, and E, represent equilibrium shapes of Cu/ZnO (recorded after about 1 hour of gas exposure), and such images are used in calculations of the interface and surface free energies.

In the images of Cu nanocrystals on ZnO, lattice fringes from both Cu and ZnO can be resolved. For ZnO, the (011) lattice spacings of 0.25 nm and the (012) spacings of 0.19 nm are readily observed. In certain instances, even spacings of about 0.14 nm corresponding to the (112) or (103) planes were seen under the high-temperature in situ conditions. For the supported Cu particles, lattice fringes with separations of 0.21 and 0.18 nm are seen. These are assigned to the Cu (111) and (200) planes, respectively. On the basis of this information and the observed angles between the terminating planes, the exposed facets of the projected particle can be identified

as the (111), (110), and (100) low-index planes (Fig. 1B). We can also determine which facet of the Cu particles is in contact with the ZnO support.

The detailed structural and morphological in situ data allow us to determine the surface free energies ( $\gamma$ ) and the work of adhesion ( $W$ ). Previously, such quantitative information could only be obtained from ex situ microscopy observations (30) or from scanning tunneling microscopy studies under ultrahigh vacuum (UHV) conditions (31). On the basis of the Wulff construction (32), we extracted the energies (Table 1) by measuring the length of the projected facets and the height of the copper particles (31). Under the imaging conditions (1.5 mbar of H<sub>2</sub> at 220°C), the hydrogen coverage on the different Cu facets is low (28), which explains the agreement with the surface free energies obtained for Cu single-crystal surfaces in vacuum (Table 1). Assuming that only low-index facets are present on the Cu particles, we can reconstruct the full three-dimensional shape of the supported Cu particle from the surface free energies in Table 1. A two-dimensional projection along the viewing direction ([011] in Fig. 1A) of the Wulff construction model (Fig. 1B) matches the observed shapes of the crystals. Image simulations with the EMS

(33) and RHODIUS (34) software packages support the assumption that the relative abundance of high-index planes is very low. In pure hydrogen, the majority of the Cu particles appear to be in contact with the ZnO support with their (111) facet, as also observed for Cu particles prepared by vapor deposition under UHV onto various atomically clean ZnO faces (35). In our case, the termination of the ZnO at the interface varies from particle to particle, indicating weak interaction and no strong preference for the Cu particles to decorate specific ZnO facets under these conditions.

The addition of water to the hydrogen gas transforms the Cu crystals into a more spherical morphology (Fig. 1C). From the projected shape, it appears that the Cu crystals are terminated by a higher fraction of (110) and (100) facets than in pure hydrogen. Hence, the (110) and (100) facets of the crystals are stabilized with respect to the (111) planes (Fig. 1D, Table 1). At the interface, however, the contact area between (111) planes of Cu and the ZnO surface is not changed substantially. This suggests that water adsorption on the different exposed Cu facets is the main driving force for the gas-induced surface reconstructions and resulting reshaping of the Cu particles.

If the H<sub>2</sub>/H<sub>2</sub>O gas mixture is replaced again by pure hydrogen, the Cu crystals revert to their original form (Fig. 2). The shape transformations were found to be reversible both when the same particles were followed during the gas changes (Fig. 2) and in measurements on a statistically significant number (~150) of randomly chosen particles after each gas treatment. Similar changes were observed for silica-supported Cu nanocrystals subjected to these gas mixtures, providing further evidence that the above changes are mainly caused by adsorption of H<sub>2</sub>O on the Cu particles.

Addition of the more reducing gas, carbon monoxide, to the hydrogen gas results in more marked changes. The Cu particles are observed to transform into disclike structures caused by an increased wetting of the ZnO support (Fig. 1E). The interfacial area increases by about 50%, suggesting a large change in interface energy. Similar changes are not observed for Cu nanoparticles on silica, suggesting a key role of the ZnO substrate. The high-resolution images show that the surface of the Cu particles on ZnO is now terminated predominantly by (111) and (100) facets with the Cu (111) facet parallel to the interface. The projected Wulff construction (Fig. 1F) was obtained by assuming that the addition of CO only changes the Cu/ZnO interface energy and not the relative Cu surface energies. This is probably a good approximation because the surface coverage of hydrogen and CO is relatively small under

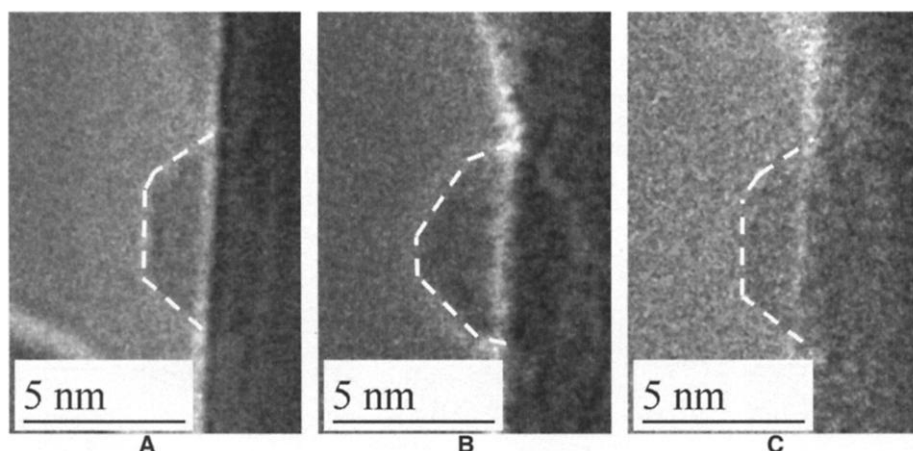


**Fig. 2.** TEM images showing the reversible shape change of a Cu nanocrystal. The same Cu nanocrystal is imaged at 220°C under (A) H<sub>2</sub> at 1.5 mbar, (B) H<sub>2</sub>:H<sub>2</sub>O (3:1) at a total pressure of 1.5 mbar, and (C) H<sub>2</sub> at 1.5 mbar.

**Table 1.** Relative surface free energies ( $\gamma_{hkl}$  and  $\gamma^*$ ) and work of adhesion ( $W$ ) for a Cu/ZnO catalyst in different gases. The values given in parentheses are surface free energies calculated for Cu single crystals in vacuum (39). All quantities are given relative to  $\gamma_{111,vac}$ , the surface free energy for the (111) facet of Cu in vacuum.  $W = 1 - \gamma^*/\gamma_{111,vac}$ , where  $\gamma_{111,vac} = 1.952 \text{ J m}^{-2}$  and  $\gamma^* = (\gamma_{interface} - \gamma_{subs})/\gamma_{111,vac}$ . The H<sub>2</sub>/H<sub>2</sub>O values are scaled assuming  $W$  to be the same as in the case of H<sub>2</sub>. The H<sub>2</sub>/CO values are scaled assuming  $\gamma_{hkl}$  to be the same as in the case of H<sub>2</sub>.

	H <sub>2</sub>	H <sub>2</sub> /H <sub>2</sub> O	H <sub>2</sub> /CO
$\gamma_{100}$	$1.08 \pm 0.03$ (1.10)	$0.61 \pm 0.03$	$1.08 \pm 0.03$
$\gamma_{110}$	$1.11 \pm 0.02$ (1.15)	$0.57 \pm 0.03$	$1.11 \pm 0.02$
$\gamma_{111}$	1	$0.59 \pm 0.02$	1
$\gamma^*$	$0.09 \pm 0.05$	$0.09 \pm 0.02$	$-0.54 \pm 0.05$
$W$	$0.91 \pm 0.05$	$0.91 \pm 0.02$	$1.54 \pm 0.05$

the conditions used here (6, 28). It has been proposed that a change in the oxidation potential of the gas may change the oxygen content in the ZnO surface and thereby the interface energy (6, 7, 28). A low oxygen content will give a strong decrease in the Cu/ZnO<sub>x</sub> interface energy because of a partial (or full) reduction of the ZnO surface layer. On the other hand, at large oxygen contents, the ZnO surface is completely oxidized (low concentration of oxygen vacancies) and the interface free energy is high.

Previously, detailed information on gas-induced structural transformation has been obtained with single-crystal model systems exposed to conditions quite far removed from those used in industrial catalysis. Thus, it has been difficult to relate the information directly to catalysis, and this has been referred to as the material and pressure gaps in catalysis (16). Our results show that insight can now be obtained at more realistic conditions and for quite complex nanoparticle systems with many different surfaces and interfaces. The observed dynamic restructuring of the catalyst also demonstrates that the relevant active sites are generated during the catalytic reaction. This further emphasizes the need for in situ studies at all the conditions that a catalyst will experience. Such studies may provide important information regarding the concentration of different type of surface sites (on low index planes, corners, steps, etc.) under various conditions (36). The structure sensitivity and dynamic morphology changes may then be incorporated into a microkinetic description of the catalytic reactions with the approach discussed earlier (28). Previously descriptions of catalysis have had to rely on assumptions regarding the nature of the exposed surfaces.

#### References and Notes

1. M. A. El-Sayed, *Acc. Chem. Res.* **34**, 257 (2001).
2. G. Ertl, H. Knözinger, J. Weitkamp, Eds., *Handbook of Heterogeneous Catalysis* (Wiley-VCH, New York, 1997), vol. 4, pp. 1856–1876.
3. A. P. Alivisatos, *Science* **271**, 933 (1996).
4. R. Jin et al., *Science* **294**, 1901 (2001).
5. J. A. Dumesic, H. Topsøe, M. Boudart, *J. Catal.* **37**, 513 (1975).
6. B. S. Clausen et al., *Top. Catal.* **1**, 367 (1994).
7. J. D. Grunwaldt, A. M. Molenbroek, N.-Y. Topsøe, H. Topsøe, B. S. Clausen, *J. Catal.* **194**, 452 (2000).
8. M. M. Günther et al., *Catal. Lett.* **71**, 37 (2001).
9. T. W. Hansen et al., *Science* **294**, 1508 (2001).
10. J. A. Dumesic, H. Topsøe, *Adv. Catal.* **26**, 121 (1977).
11. B. S. Clausen, H. Topsøe, R. Frahm, *Adv. Catal.* **42**, 315 (1998).
12. J. M. Thomas, G. A. Somorjai, Eds., *Topics in Catalysis*, vol. 8 (Balzer Science Publishers BV, Bussum, the Netherlands, 1999).
13. G. A. Somorjai, *Cattech* **3**, 84 (1999).
14. J. W. Niemantsverdriet, *Spectroscopy in Catalysis* (Wiley-VCH, Weinheim, Germany, 2000).
15. C. T. Campbell, *Science* **294**, 1471 (2001).
16. N. I. Jaeger, *Science* **293**, 1601 (2001).
17. D. A. Jefferson, P. J. F. Harris, *Nature* **332**, 617 (1988).
18. R. M. Stockman, H. W. Zandbergen, A. D. Langeveld, J. A. Moulijn, *J. Mol. Catal. A Chem.* **102**, 147 (1995).
19. J. Urban, H. Sack-Kongehl, K. Weiss, *Catal. Lett.* **49**, 101 (1997).

20. A. K. Datye, in *Handbook of Heterogeneous Catalysis*, G. Ertl, H. Knözinger, J. Weitkamp, Eds. (Wiley-VCH, New York, 1997), vol. 2, pp. 493–512.
21. J. M. Thomas, *Angew. Chem. Int. Ed.* **38**, 3588 (1999).
22. R. T. Baker, P. S. Harris, *J. Phys. E Sci. Instrum.* **5** (no. 8), 793 (1970).
23. P. L. Gai, E. Boyes, *Ultramicroscopy* **67**, 219 (1997).
24. J. B. Hansen, in *Handbook of Heterogeneous Catalysis*, G. Ertl, H. Knözinger, J. Weitkamp, Eds. (Wiley-VCH, New York, 1997), vol. 4, pp. 1856–1876.
25. J. R. Rostrop-Nielsen, *Phys. Chem. Chem. Phys.* **3**, 283 (2001).
26. N.-Y. Topsøe, H. Topsøe, *J. Mol. Catal. A Chem.* **141**, 95 (1999).
27. F. Boccuzzi, G. Ghiotti, A. Chiorino, *Surf. Sci.* **156**, 933 (1985).
28. C. V. Ovesen et al., *J. Catal.* **168**, 133 (1997).
29. The ZnO support was prepared by flame synthesis in order to obtain well-developed crystals (37). Stöber spheres of diameter 600 to 700 nm were used as silica support (38). After impregnation and drying, the catalysts were heated in 2% O<sub>2</sub> in N<sub>2</sub> at 400°C for 4 hours.
30. C. R. Henry, *Surf. Sci. Rep.* **31**, 231 (1998).
31. K. H. Hansen et al., *Phys. Rev. Lett.* **83**, 4120 (1999).
32. G. Wulff, *Z. Kristallogr.* **34**, 449 (1901).
33. P. Stadelmann, *Ultramicroscopy* **21**, 131 (1987).
34. S. Bernal et al., *Ultramicroscopy* **72**, 135 (1998).
35. C. T. Campbell, *Surf. Sci. Rep.* **27**, 1 (1997).
36. J. B. Wagner, P. L. Hansen, S. Helveg, B. S. Clausen, N.-Y. Topsøe, H. Topsøe, in preparation.
37. J. R. Jensen, T. Johannesen, S. Wedel, H. Livbjerg, *J. Nanoparticle Res.* **2** (no. 4), 363 (2000).
38. W. Stöber, A. Fink, E. Bohn, *J. Colloid Interface Sci.* **26**, 82 (1968).
39. L. Vitos, A. V. Ruban, H. L. Skriver, J. Kollár, *Surf. Sci.* **411**, 186 (1998).
40. We would like to thank K. Højrup Hansen, E. Johnson, C. V. Ovesen, A. Datye, and N.-Y. Topsøe for fruitful discussions; T. Johannesen for supply of the flame-synthesized ZnO<sup>37</sup>; and H. Teunissen for preparation of the catalysts. Haldor Topsøe, H.-J. Hansen, and W. T. Liu are gratefully acknowledged for keen interest in the establishment of the microscope facility, and the China Technical Consultants Foundation is thanked for financial participation. J.B.W. would like to thank the Danish Research Academy for supporting a scholarship at the Interdisciplinary Center of Catalysis (ICAT). S.H. acknowledges support from the Danish Research Council, STVF, through an extension of its materials development program. The FEI company is thanked for fruitful collaboration on the development of the in situ TEM.

26 December 2001; accepted 14 February 2002

## Lateral Hopping of Molecules Induced by Excitation of Internal Vibration Mode

T. Komeda,<sup>1</sup> Y. Kim,<sup>1</sup> Maki Kawai,<sup>1\*</sup> B. N. J. Persson,<sup>2</sup> H. Ueba<sup>3</sup>

We demonstrate electron-stimulated migration for carbon monoxide (CO) molecules adsorbed on the Pd(110) surface, which is initiated by the excitation of a high-frequency (HF) vibrational mode (C–O stretching mode) with inelastic tunneling electrons from the tip of scanning tunneling microscopy. The hopping phenomenon, however, cannot be detected for CO/Cu(110), even though the hopping barrier is lower than in the CO/Pd(110) case. A theoretical model, which is based on the anharmonic coupling between low-frequency modes (the hindered-translational mode related to the lateral hopping) and the HF mode combined with electron-hole pair excitation, can explain why the hopping of CO is observed on Pd(110) but not on Cu(110).

The diffusion of adsorbed species on surfaces can be controlled thermally to some extent. The nonthermal control of surface migration of adsorbates (using electron excitation) could have many applications. Only a few studies have shown that electron irradiation can induce nonthermal transfer of surface species (1, 2), a process called electron-stimulated migration (ESM). Atoms can be manipulated with the scanning tunneling microscope (STM) (3), and excitation of the adsorbate-substrate vibrational mode induces various surface phenomena such as desorption (4), dissociation (5), and rotation of adsor-

bates (6). For example, the rotation of C<sub>2</sub>H<sub>2</sub> on Cu is enhanced with the excitation of C–H stretching vibrational mode (7). However, the detailed mechanism of the coupling between the rotation of the molecule and the vibrational mode is still an open question. Here, we demonstrate ESM caused by tunneling electrons for CO molecules adsorbed on Pd(110), which is initiated by the excitation of a high-frequency (HF) vibrational mode (C–O stretching mode, ~240 meV). The hopping phenomenon, however, cannot be detected for CO/Cu(110) in spite of the much lower hopping barrier than for CO/Pd(110). The underlying mechanism is examined by a theoretical calculation that includes anharmonic coupling between low-frequency (LF, ~25 meV) modes (the hindered-translational mode related to the lateral hopping) and the HF mode, as well as the vibrational damping of the HF mode caused by electron-

<sup>1</sup>RIKEN, 2-1 Hirosawa, Wako, Saitama, 351-0198, Japan. <sup>2</sup>IFF, FZ-Jülich, 52425, Jülich, Germany. <sup>3</sup>Department of Electronics, Toyama University, Gofuku, Toyama, Japan.

\*To whom correspondence should be addressed. E-mail: maki@postman.riken.go.jp